Wireless Concrete Mixture Composition Sensor Based on Time-Coded UWB RFID

Angel Ramos, *Student Member, IEEE*, David Girbau, *Senior Member, IEEE*, Antonio Lazaro, *Member, IEEE*, and Ramon Villarino

***Abstract*—This work presents a non-destructive wireless, concrete quality sensor based on chipless ultra-wideband radio frequency identification. The sensor is based on detecting the delay between two scattering modes induced by permittivity changes in the concrete. Theoretical, simulated and measured results with several embedded tags in samples are shown. The composition of the concrete blocks is remotely detected and classified.**

***Index Terms*—Concrete, multilayer microstrip, non-destructive testing (NDT), permittivity sensor, RFID, UWB.**

I. Introduction

STRUCTURAL health of concrete-based civil structures is a major concern in today's society [1]. Unexpected events such as earthquakes, hurricanes, or simply a material deterioration because of a wrong mixture of compounds, could cause a structure to collapse. During the construction period, samples of the construction compounds are usually inspected. However, long-term non-destructive testing (NDT) of the civil structure is also desired. In this context, several works have been presented recently, with the aim of wirelessly sense these structures. Battery-powered active sensors, using microcontrollers and accelerometers are reviewed in [1]. A passive permittivity sensor which uses UHF radiofrequency identification (RFID) at 870 MHz is presented in [2]. Another UHF RFID sensor is presented to detect the permittivity of lightweight concrete in [3]. The dielectric constant of concrete is obtained in [4] by measuring the deflection and loss of electromagnetic waves in concrete blocks using a continuous wave (CW) radar.

This work aims to classify the mixture composition of concrete from its permittivity using chipless time-coded ultra-wideband (UWB) RFID tags [5]. UWB has good penetration in materials and UWB antennas, on the contrary to narrowband antennas, do not suffer from critical detuning. Since chipless tags do not require any electronics, the costs can be drastically reduced in large-scale applications, and their lifetime is very long. The tags are partly embedded inside concrete, avoiding contact problems between the tag and the material, which could lead to unreliable measurements (due to the material roughness).

The letter is organized as follows. Section II presents the time-domain UWB RFID theory, the sensor design and the multilayer microstrip permittivity theory. Section III presents a method to calibrate the tag and shows the measured results. Finally, Section IV provides the conclusions.

Manuscript received March 04, 2015; revised May 06, 2015; accepted July 01, 2015. This work was supported by the Spanish Government under Project TEC2011-28357-C02-01, the AGAUR under Grant FI-DGR 2012, and the European H2020 under Grant Agreement 645771-EMERGENT.

The authors are with the Department of Electronic, Electric and Automatic Control Engineering, Universitat Rovira i Virgili, Tarragona 43007, Spain (e-mail: david.girbau@urv.cat).

Color versions of one or more of the figures in this paper are available online at http://ieeexplore.ieee.org.

Digital Object Identifier 10.1109/LMWC.2015.2463105

II. Theory

A. Tag-Reader System

Fig. 1(a) shows a scheme of the system. The sensor tag can be seen as an equivalent two-port network (antenna) loaded with an open-ended delay line of length L and characteristic impedance Z_c. In this case, a Vivaldi antenna and a meandered microstrip delay line. The delay line is embedded in concrete, as shown in both the layouts [Fig. 1(b)] and photographs [Fig. 1(c)]. The reader sends through its transmitting (Tx) antenna a Gaussian pulse $p(t)$ which hits the tag. The signal at the reader's receiving (Rx) antenna in time domain can be approximated as the sum of several peaks (1) [see Fig. 1(a)]

$$s(t) = s_{\mathrm{Coupl.}}(t) + s_{\mathrm{Clutter}}(t) + s_{\mathrm{Str.}}(t) + s_{\mathrm{Plate}}(t) + s_{\mathrm{Concrete}}(t) + s_{\mathrm{Tag}}(t) \quad (1)$$

where $s_{\mathrm{Coupl.}}$ is the coupling from the reader Tx to Rx antenna and s_{Clutter} is the clutter from the scene. Both can be removed by using a background subtraction technique. $s_{\mathrm{Str.}}$ corresponds to the tag structural mode, which depends on the tag shape, size and material. A Vivaldi antenna has a small radar cross-section (RCS) in its optimum radiation pattern Azimuth angle. Therefore, its structural mode is small and difficult to detect. A metal plate is soldered in the Vivaldi ground plane in perpendicular to the Vivaldi ground plane, providing a strong reference peak. This plate is separated from the tapered transition so it does not affect the antenna. s_{Plate} corresponds to the signal backscattered at the metal plate, s_{Concrete} corresponds to the reflection at the concrete slab or wall. Finally, s_{Tag} corresponds to the tag mode, which depends on the load of the antenna (here an open-ended delay line) s_{Tag} is the part of $p(t)$ that propagates inside the tag and is reradiated to the reader with the information of the material where the line is embedded.

The Vivaldi antenna has been chosen because it permits to integrate a long meander delay without having undesired effects. Also, with other antennas such as UWB monopoles, increasing the ground plane size (to fit a long delay) worsens their performance [6]. Finally, with a Vivaldi antenna the gain is larger than UWB monopoles and its boresight is perpendicular to the

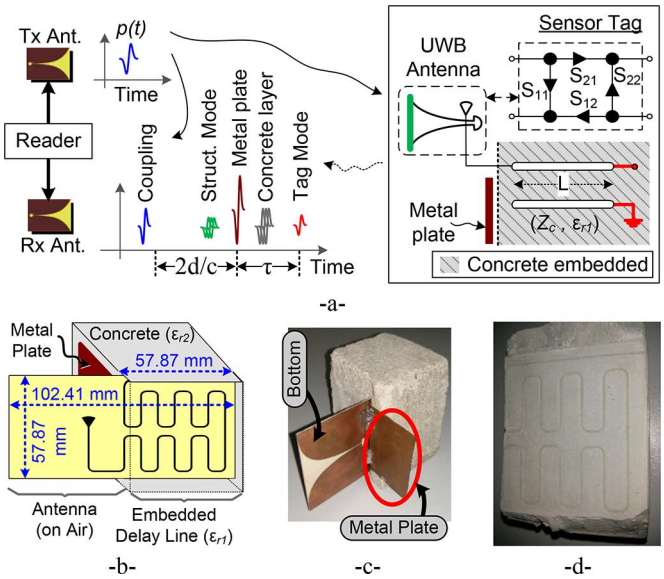

Fig. 1. (a) Scheme of the tag-reader system. (b) Scheme of the embedded designed tag, top face. (c) Photograph of the embedded tag, back face. (d) Cut of the concrete layer after fabrication.

concrete wall or slab. As shown in Fig. 1(a), the signals corresponding to $s_{\mathrm{Str.}}$ and s_{Concrete} are unstable in time, because of changes in angle or distance from one measurement to another, and because of dispersion, respectively. Therefore, s_{Plate} is used as reference, which also denotes the limit where the tag should be embedded in concrete. The delay between s_{Plate} and s_{Tag} is addressed as τ. τ depends on the delay line length L and the propagation speed of the medium v, which, in turn, depends on the effective permittivity of the medium $\varepsilon_{\mathrm{efr}}$. $\varepsilon_{\mathrm{efr}}$, in turn, depends on the permittivities of both the substrate (ε_{r1}) and the concrete slab (ε_{r2}). Finally, the term *2d/c* accounts for the distance between the tag and the reader, from which τ is independent of.

B. Multilayer Microstrip Permittivity

Fig. 2(a) shows a scheme of the multilayer microstrip structure that models the situation. The RO4003C substrate permittivity is $\varepsilon_{r1} = 3.55$, and its height is $h = 0.813$ mm. The delay line width is $w = 0.7$ mm (which corresponds to a characteristic impedance $Z_C = 80\ \Omega$ with the tag in free space). The permittivity ε_{r2} corresponds to the concrete added on contact with the delay line. Using the conformal mapping method proposed in [7], the effective permittivity $\varepsilon_{\mathrm{efr}}$ of the multilayer microstrip structure can be obtained

$$\varepsilon_{\mathrm{efr}} = \varepsilon_{r1} q_1 + \varepsilon_{r2} \frac{(1-q_1)^2}{\varepsilon_{r2}(1-q_1-q_2)+q_2} \qquad (2)$$

where q_1 and q_2 are the filling factors defined in [7]. In order to study the effect of the concrete thickness, Fig. 2(b) shows $\varepsilon_{\mathrm{efr}}$ as a function of ε_{r2} and h_2 (with a fixed h). ε_{r2} is swept from 1 to 5. It can be observed that, for heights greater than 8 mm, $\varepsilon_{\mathrm{efr}}$ only depends on ε_{r2}. In civil engineering, the concrete layer is thicker than 8 mm. Therefore, the concrete thickness is not needed to be known in a real situation.

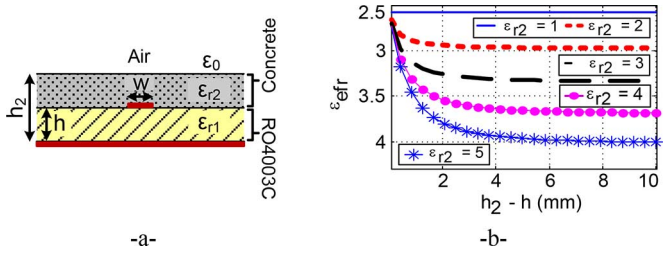

Fig. 2. (a) Scheme of the multilayer microstrip structure. (b) Calculated medium permittivity $\varepsilon_{\mathrm{efr}}$ as a function of the concrete layer permittivity ε_{r2} and thickness $(h_2 - h)$.

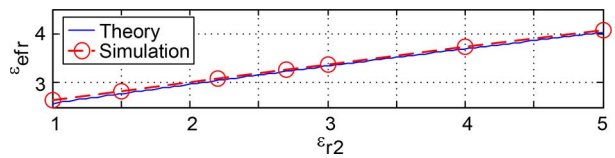

Fig. 3. Theoretical and simulated effective permittivity of the multilayer structure.

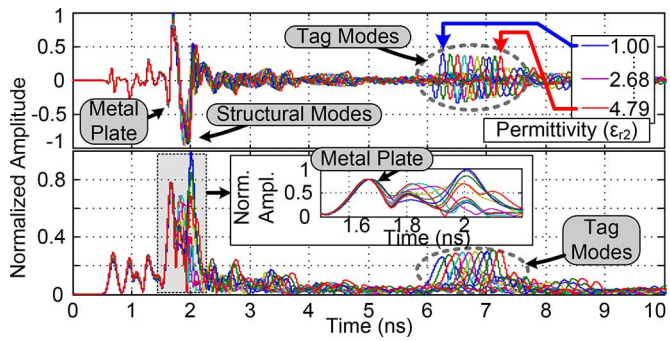

Fig. 4. Simulated time-domain signal of the tag for ε_{r2} from 1 to 5. (top) RAW signal. (bottom) Signal after applying the CWT.

To validate the theory, the S parameters of a multilayer microstrip transmission line of width $w = 0.7$ mm on RO4003C have been simulated with Agilent Momentum. The structure follows the scheme of Fig. 2(a), where the concrete layer height is $h_2 - h = 10$ mm and ε_{r2} is swept from 1 to 5. Fig. 3 shows a comparison between the theoretical [from (2)] and simulated effective permittivity of the multilayer structure. A nearly-linear behaviour is obtained with both theory and simulations.

III. Results

The full tag [see Fig. 1(b)] is now simulated using Ansys HFSS. A 10-mm thick concrete block is added on top of the tag delay line. The permittivity of this block (ε_{r2}) is again swept from 1 to 5, with 20 samples within the range. Fig. 4 shows the simulated time-domain signal before and after applying the Continuous Wavelet Transform (CWT) [5]. It is important to note that not all the samples of ε_{r2} are shown for representation convenience. The metal plate fixes the time reference, while the tag mode varies depending on ε_{r2}.

The Time Domain PulsON P400 MRM impulse radar is used as the reader in the measurements. A background subtraction technique (scene without the tag) is applied for all measurements, as well as the CWT [5]. In the case of concrete walls, the

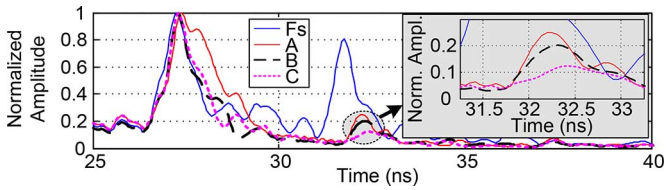

Fig. 5. Measured time-domain response of the tag embedded in three concrete blocks and on air after applying the CWT.

TABLE I
CONCRETE BLOCKS COMPOSITION AND PERMITTIVITY

Block	% C	% S	$\bar{\tau}$ (ns) $\pm$ σ	Meas. ε_{r2}	Ref. ε_{r2} (CRR)
A	25	75	5.000	3.56	3.51
B	50	50	5.070	3.98	4.07
C	100	0	5.125	4.31	4.24

% C: Percentage of Concrete, % S: Percentage of Sand, σ = 30 ps

tags are embedded and cannot be removed, and then the background can be obtained from a portion of the wall without tag. It is important to note that in this case the reader has to be at the same distance and angle for a proper background measurement.

For any given measurement, the delay τ [see Fig. 1(a)] between the reflection at the perpendicular metal plate and the tag mode can be modeled as

$$\tau = \tau_0 + 2L_{\text{eff}}\sqrt{\varepsilon_{\text{efr}}}/c \tag{3}$$

where τ_0 accounts for a constant delay offset between the metallic plate and the delay line, c is the speed of light in vacuum and L_{eff} is the equivalent electrical delay line length. τ_0 and L_{eff} are unknown, and have to be experimentally determined as first-step calibration parameters. To do so:

a) The tag is measured in free space ($\varepsilon_{r2} = 1$) and with an attached 10 mm PTFE slab (known stable material, $\varepsilon_{r2} = 2.2$), using background subtraction and CWT.
b) The equivalent ε_{efr} for free space and PTFE are obtained from the theoretical (or simulated) curve of Fig. 3.
c) Using the measured delays from a), equivalent permittivities from b), and (3), $L_{\text{eff}} = 0.27$ m and $\tau_0 = 1.571$ ns are obtained. These parameters are stored as calibration, can be measured outside of the construction field, and they work at any distance between tag and reader.

In order to experimentally validate the sensor tag, three concrete blocks (A, B and C) are fabricated, embedding an identical tag in each block. The blocks are composed by a mixture of portland concrete and sand. The compositions are depicted in Table I. The blocks have been dried in still air for four weeks before measuring them. Three sets of 100 measurements have been performed at a 40 cm tag-reader distance. A block without any tag embedded is used to emulate the real-case background (portion of wall without tag). Fig. 5 shows the measured time-domain response of the blocks. The mean delays $\bar{\tau}$ between the metal plate and the tag modes are shown in Table I. The tag mode amplitude is reduced when the tag is embedded in concrete but the peaks and the time difference can still be perfectly detected. Using (3) with the calibration parameters ($L_{\text{eff}} = 0.27$ m and $\tau_0 = 1.571$ ns) and $\bar{\tau}$ from Table I, ε_{efr} can be obtained, and ε_{r2} is derived by inverting Fig. 3.

The permittivity of dry sand is between 2.5 and 2.75 [8]. The permittivity of concrete is around 5 [3], [4]. Therefore, the estimated ε_{r2} falls within the expected range for the mixtures. To validate these measurements, the permittivities of the samples are also measured using a microstrip circular ring resonator (CRR) [9] and an Agilent E8364C Vector Network Analyzer. These results are also shown in Table I. A good agreement is observed. It is important to note that, because of the radar time resolution (±30 ps), there is an error in ε_{r2} about ±0.1. As shown in (3), the permittivity depends on a square root term. Therefore, there is more sensitivity for smaller permittivities, i.e., when the part of sand increases. In comparison with the chip-based UHF RFID systems proposed in [2], [3], the tag does not use a chip, which would reduce costs in a large-scale application; however a background subtraction is required, which is not required in chip-based systems. In comparison with [4], the sensor proposed here permits to measure the permittivity without previously knowing the concrete slab depth. Also, it is not required to detect a metal on the other side of the slab or wall, which could be difficult for very thick walls due to loss.

IV. CONCLUSION

This work has presented a chipless concrete mixture composition sensor based on UWB RFID. It is based on the dependence of the permittivity of concrete on the mixture composition. The results show that it is possible to remotely detect the mixture of concrete and sand in a concrete block by using UWB technology for classification purposes and long-term quality evaluation.

REFERENCES

[1] J. P. Lynch, "An overview of wireless structural health monitoring for civil structures," *Phil. Trans. R. Soc. A*, vol. 365, no. 1851, pp. 345–372, 2007.
[2] G. Marrocco, L. Mattioni, and C. Calabrese, "Multiport sensor RFIDs for wireless passive sensing of objects—Basic theory and early results," *IEEE Trans. Antennas Propag.*, vol. 51, no. 1, pp. 31–39, 2003.
[3] R. Suwalak, C. Phongcharoenpanich, D. Torrungrueng, and M. Krairiksh, "Determination of dielectric property of construction material products using a novel RFID sensor," *Progress Electromag. Res.*, vol. 130, pp. 601–617, 2014.
[4] X. Hui, L. Bangyu, X. Shaobo, and F. Hongzhuan, "The measurement of dielectric constant of the concrete using single-frequency CW radar," in *Proc. 1st Int. Conf. Intell. Netw. Intell. Syst.*, 2008, pp. 588–591.
[5] A. Lazaro, A. Ramos, D. Girbau, and R. Villarino, "Chipless UWB RFID tag detection using continuous wavelet transform," *IEEE Antennas Wireless Prop. Lett.*, vol. 10, pp. 520–523, 2011.
[6] Y. Lu, Y. Huang, H. T. Chatta, and P. Cao, "Reducing ground-plane effects on UWB monopole antennas," *IEEE Antennas Wireless Propag. Lett.*, vol. 10, pp. 147–150, 2011.
[7] J. Svacina, "A simple quasi-static determination of basic parameters of multilayer microstrip and coplanar waveguide," *IEEE Microw. Guided Wave Lett.*, vol. 2, no. 10, pp. 385–387, 1992.
[8] C. Matzler, "Microwave permittivity of dry sand," *IEEE Trans. Geos. Remote Sens.*, vol. 36, no. 1, pp. 317–319, Jan. 1998.
[9] P. A. Bernard and J. M. Gautray, "Measurement of dielectric constant using a microstrip ring resonator," *IEEE Trans. Microw. Theory Tech.*, vol. 39, no. 3, pp. 592–595, 1991.